Inorg. Chem. **2005**, *44*, 5092–5103

The Stability and Eventual Lone Pair Distortion of the Hexahalide Complexes and Molecules of the Fifth to Eighth Main-Group Elements with One Lone Pair, as Isolated Entities or in Oligomeric Clusters: A Vibronic Coupling and DFT Study

Mihail Atanasov[†,‡] **and Dirk Reinen***[,†]

Fachbereich Chemie, Universität Marburg, Hans-Meerwein Strasse, D-35032 Marburg, Germany, Bulgarian Academy of Sciences, and Institute of General and Inorganic Chemistry, 1113 Sofia, Bulgaria

Received December 1, 2004

The introduced DFT-supported vibronic coupling model together with the hardness rule indicates, for the title compounds, that the tendency toward lone pair (LP) distortions decreases with increasing coordination number (CN) and upon proceeding from fluoride to iodide as the ligands. Thus, only some hexafluoro complexes and molecules are calculated to actually undergo LP deformations; here, from the possible highest-symmetry deformations, those with C_{4v} geometry possess the lowest energy, leading to the complete ablation of one ligand and, hence, explaining the nonexistence of the complexes AsF_6^{3-}, SbF_6^{3-}, and SF_6^{2-}. If a lower-symmetry strain is imposed on the octahedral species, for example, induced by the simultaneous presence of terminal and bridging ligands in oligomers, the vibronic energy potential is activated. It may induce pronounced distortions, which are much larger than those of analogous clusters with central ions lacking the LP. Dimers and tetramers with common edges and faces are investigated, with the predicted and calculated deformations of the constituting octahedra again following the stability sequence $C_{4v} > C_{2v} > C_{3v}$. The model nicely accounts for the observed trends, as well as reproduces the experimental structures and energy balances, at least semiquantitatively; its predictive power exceeds that of the valence-shell electron-pair repulsion concept.

I. Introduction

It has long been a permanent point of discussion as to why polyhedra of lower coordination numbers (CNs) with lone-pair (LP) cations show the kinds of distortion predicted by the VSEPR (valence-shell electron-pair repulsion) model of Gillespie and Nyholm,[1,2] whereas, for example, the LP remains mostly stereochemically inactive in isolated complexes of CN = 6, the latter usually remaining in their nearly or completely undistorted octahedral parent geometry. Such species, either as monomers or oligomers with partly bridging ligands, will be studied in this contribution. We have already investigated a series of halide complexes with lower CNs, centered by atoms from the fifth to eighth main group of the periodic system of elements (PSE) with *one* LP (A^{III}, P to Bi; B^{IV}, S to Te; C^{V}, Cl to I; Xe^{VI}). In analyzing the respective geometric and energetic situation, we used a vibronic-coupling-type concept, which differed from conventional and well-established approaches[3] in various aspects.[4−7] This model, which offers many advantages with respect to the VSEPR approach and has, as well, predictive power in regard to whether a LP complex undergoes a distortion or not, is shortly portrayed in the next section. In particular, it is deduced that the LP effect follows the chemical hardness of the considered molecule or complex (*hardness rule*),[4,6,7] this concept partly following early ideas

* Author to whom correspondence should be addressed. E-mail: reinen@chemie.uni-marburg.de. Fax: 06421-2828917.
† Universität Marburg.
‡ Bulgarian Academy of Sciences.

(1) Gillespie, R. J.; Nyholm, R. S. *Q. Rev., Chem. Soc.* **1957**, *11*, 339.
(2) Gillespie, R. J.; Popelier, P. L. A. *Chemical Bonding and Molecular Geometry*; Oxford University Press: New York, 2001.
(3) Öpik, U.; Pryce, M. H. L. *Proc. R. Soc. London, Ser. A* **1957**, *238*, 425. Bader, R. F. W. *Can. J. Chem.* **1962**, *40*, 1164. Pearson, R. G. *J. Am. Chem. Soc.* **1969**, *91*, 4947. Bersuker, I. B. *Chem. Rev.* **2001**, *101*, 1067.
(4) Atanasov, M.; Reinen, D. *J. Am. Chem. Soc.* **2002**, *124*, 6693.
(5) Atanasov, M.; Reinen, D. *Adv. Quantum Chem.* **2003**, *44*, 355.
(6) Atanasov, M.; Reinen, D. *Inorg. Chem.* **2004**, *43*, 1998.
(7) Atanasov, M.; Reinen, D. *J. Phys. Chem. A* **2001**, *105*, 5450.

10.1021/ic040125v CCC: $30.25
Published on Web 06/17/2005

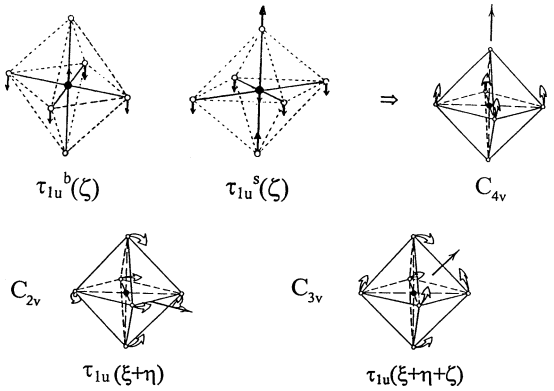

Figure 1. Highest symmetry ζ components of the two vibronically active τ_{1u} vibrations (s = stretching and b = bending) in O_h (CN = 6), leading into C_{4v} with one axial ligand at a large bond distance. The linear combinations of the τ_{1u} components with the highest displacement symmetries besides C_{4v} are also shown (C_{3v}, C_{2v}); here, the arrows mark the directions opposite of the LP orientation.

of R. G. Pearson.[8] *A LP species becomes the softer and, hence, the less susceptible to distortions the higher the CN and the larger and more polarizable the halide ion (X^-: $F^- \rightarrow I^-$) becomes*. Concerning the central LP atoms, the sequence of decreasing hardness does not necessarily follow the PSE (A^{III}, P → Bi; B^{IV}, S → Se ≈ Te; C^{V}, I → Cl ≈ Br) and is only distinct in the case of the fluoride species.[6]

Sometimes the vibronic instability, if supported by the *ionic radii effect*,[4,6] may lead to the repulsion of *one* ligand toward a large bond distance or even to the complete ablation of the respective halide ion. This effect, which is a familiar concept in solid-state chemistry, predicts a decrease of the CN if the ionic radii ratio $q = r$ (cation)/r (anion) becomes smaller than certain limiting values.[9] Thus, for example, the $P^{III}Cl_4^-$ and $P^{III}Br_4^-$ complexes do not exhibit the expected butterfly geometry with two long- and two short-bonded ligands ($T_d \rightarrow C_{2v}$) but possess a lower-symmetry C_s shape,[10] which is intermediate between the C_{2v} one and a structure near to C_{3v}, characteristic for PCl_3 and PBr_3, with one additional halide anion at a very large bond distance.[4,6] A similar phenomenon is expected for CN = 5. Here, the C_s distortion pathway aims at a geometry in which one ligand moves toward a long distance from the coordination center, leaving the other four ligands essentially as observed in the butterfly structure for CN = 4. Such steric behavior is predicted for the $P^{III}Cl_5^{2-}$ complex.[6]

In the context of this investigation, we emphasize that the ionic radii effect also has supporting influence in the case of CN = 6. The highest symmetry distortions predicted for the latter CN are induced by ligand displacements leading into the point groups C_{4v}, C_{2v}, and C_{3v} (Figure 1). The result of our study is that, for example, the complex $Sb^{III}F_6^{3-}$ should undergo pronounced ligand displacements according to C_{4v}, such that the ligand in the LP direction leaves the complex completely.[4] *Apparently, the nonexistence of the $Sb^{III}F_6^{3-}$ complex is essentially a vibronic LP effect*. The latter polyhedron is unstable with respect to $Sb^{III}F_5^{2-}$ and a single F^- anion, whereby the *complete* ablation of the latter ligand has to be attributed to the supporting influence of the ionic radii effect.

We will deal with the steric and energetic consequences of the presence of *one* LP in (isolated) octahedral complexes in Section III. In Section IV, we will treat cases with CN = 6, in which the complexes do not appear as isolated species but where two or more ligands are shared between two or more coordination centers. Such geometric patterns represent effective lower-symmetry strains, which may activate a finite vibronic energy increment and induce pronounced distortions beyond those expected for complexes without LP, this occurring even in cases where otherwise (as isolated species) regular octahedral shapes are expected. Weak strains from the higher-order coordination sphere,[11] usually acting on complexes imbedded in a lower-symmetry crystal structure, may also induce distinct polyhedron distortions.

We can nicely reproduce, at least semiquantitatively, the regular shapes or only weak distortions of (more or less isolated) complexes and polyhedra such as $Se^{IV}F_6^{2-}$, $Cl^{V}F_6^-$, $Br^{V}F_6^-$, $I^{V}F_6^-$, and $Xe^{VI}F_6$, on one hand, and the pronounced deformations in interconnected polyhedron clusters such as $Se^{IV}(Te^{IV})_2X_{10}^{2-}$, $Se^{IV}(Te^{IV})_2X_9^-$ (X^- = Cl, Br, I), and so forth, on the other hand, where structural data are available from the experiment.[12−16] We present evidence that our DFT-supported vibronic coupling concept has the potential to provide a basic understanding of the observed structural and energetic properties of LP complexes and molecules with higher CNs, such as CN = 6, where the VSEPR model finds its limit.

II. Theory

II. 1. The Vibronic Coupling Model—General. The vibronically active normal modes, initiating LP distortions, are easily evaluated by group theory, and the corresponding τ_2-distortion pathways are exemplarily illustrated for CN = 4 in Figure 2, representing an $A_1 \otimes \tau_2 \otimes T_2$ pseudo Jahn Teller (PJT) interaction.[3,4,6] Whereas in the high-symmetry parent geometry the ground-state implies the LP being of s^2 type, the symmetry-lowering during distortion allows for the mixing with an excited s^1p^1-type state, thus imparting directional properties to the (beforehand, spherically symmetric) LP. Figure 2 depicts, as a model example, the potential curve of $Te^{IV}F_4$ in comparison to that of $Sn^{IV}F_4$ without the LP. The (symmetry-equivalent) minima along the τ_2 distortion path in the former case visualize the energy gain E_{-m} when following the deformation from the tetrahedron (T_d) structure to the butterfly-shaped C_{2v} structure. According to our vibronic model,[4,6,17] E_{-m}

(8) Pearson, R. G. *Science* **1966**, *151*, 172.
(9) Wells, A. F. *Structural Inorganic Chemistry*, 5th ed.; Clarendon Press: Oxford, 1984; Chapter 3.
(10) Dillon, K. B.; Platt, A. W. G.; Schmidpeter, A.; Zwaschka, F.; Sheldrick, W. S. *Z. Anorg. Allg. Chem.* **1982**, *488*, 7. Sheldrick, W. S.; Schmidpeter, A.; Zwaschka, F.; Dillon, K. B.; Platt, A. W. G.; Waddington, T. C. *J. Chem. Soc., Dalton Trans.* **1981**, 413.
(11) Atanasov, M.; Reinen, D. *Comprehensive Coordination Chemistry II, Vol. 1 Fundamentals*; Lever, A. B. P., Ed.; Elsevier: New York, 2003; Chapter 1.36.
(12) Mahjoub, A. R.; Zhang, X.; Seppelt, K. *Chem.—Eur. J.* **1995**, *1*, 265. Mahjoub, A. R.; Hoser, A.; Fuchs, J.; Seppelt, K. *Angew. Chem.* **1989**, *101*, 1528.
(13) Christe, K. O.; Wilson, W. W.; Chrakal, R. V.; Sanders, C. P.; Schrobilgen, G. J. *Inorg. Chem.* **1990**, *29*, 3506.
(14) Mahjoub, A. R.; Seppelt, K. *Angew. Chem.* **1991**, *103*, 309.
(15) Seppelt, K.; Lentz, D. *Prog. Inorg. Chem.* **1982**, *29*, 167.
(16) Krebs, B.; Ahlers, F.-P. *Adv. Inorg. Chem.* **1990**, *35*, 235.

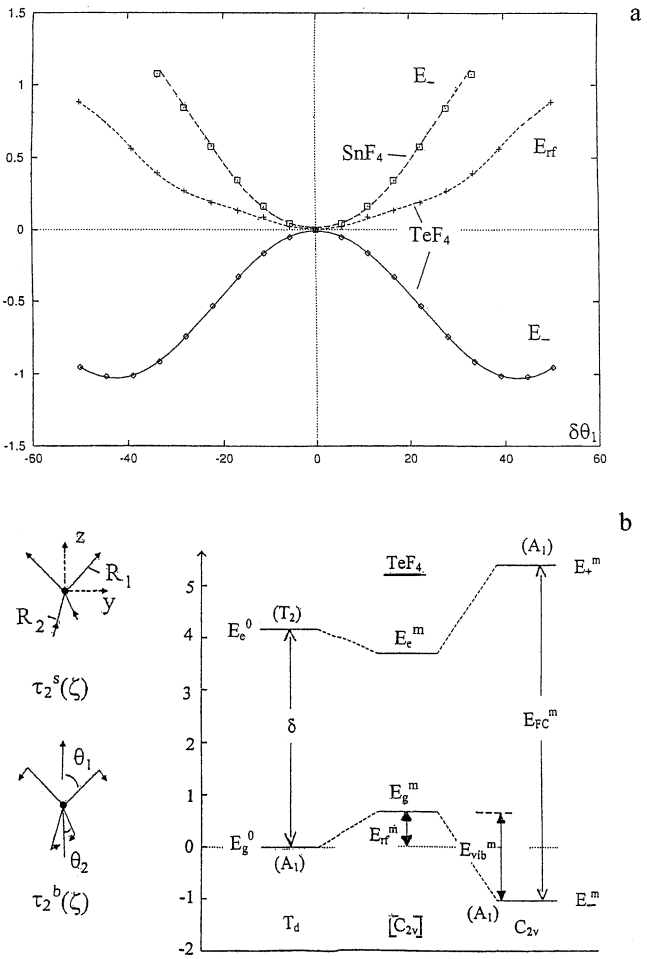

Figure 2. Potential energy curves of $Te^{IV}F_4$ and $Sn^{IV}F_4$ along the τ_2 ($T_d \rightarrow C_{2v}$) distortion path, E_- (eV) dependent upon the angular change $\delta\theta_1 = \theta_1 - 54.73$ (in degrees), with every point for TeF_4 corresponding to a full DFT optimization at the chosen θ_1 angle (in the case of SnF_4, the same geometries with an average bond length correction of −0.08 Å were chosen); the restoring energy (see eqs 1, 6, and 9) for TeF_4 is also depicted (a). The energy diagram of $Te^{IV}F_4$ in T_d and C_{2v} with the (hypothetical) intermediate situation according to $E_{vib}{}^m = 0$ (in brackets) is shown in part b; the symmetries of the interacting states are indicated (in parentheses). $E_{FC}{}^m$ denotes the Franck−Condon transition between the symmetry-equivalent many-electron $A_1(\approx ...s^2)$ and $A_1(\approx ...s^1p_z^1)$ states in C_{2v}, and δ denotes the initial splitting in T_d. The higher-symmetry ζ components of the two vibronically active τ_2 vibrations (b = bending and s = stretching) in T_d (CN = 4), leading into the butterfly-shaped C_{2v} geometry ($2\theta_1 > 109{,}47° > 2\theta_2$. $R_1 > R_2$), are illustrated as well.

can be looked at as being composed of two increments, the restoring and the vibronic energy contributions, $E_{rf}{}^m$ and $E_{vib}{}^m$, respectively: $E_{rf}{}^m$ is the total energy afforded to distort the complex, but without

$$E_-{}^m = E_{rf}{}^m - E_{vib}{}^m \qquad (1)$$

taking the vibronic mixing between s- and p-type orbitals and states into account, and is usually positive in sign. $E_{vib}{}^m$ is the energy gain solely due to this mixing effect and, hence, is a *purely orbital quantity*. The energy diagram in Figure 2 illustrates such a compositional analysis of the vibronic interaction between the A_1 ($...s^2$) ground state and the T_2 ($...s^1p^1$) excited state for the tetrahedral TeF_4 molecule. The upper index m indicates that the respective parameter refers to the DFT optimization occurring at the *minimum position of the distorted geometry*. In contrast to $E_-{}^m$, $E_{rf}{}^m$ and $E_{vib}{}^m$ are basically model quantities characterizing a hypothetical situation. $E_{vib}{}^m$ embodies, as the essential component, the nondiagonal matrix element N^m, which mediates the orbital s−p mixing. *Because N^m is directly reflected by the chemical hardness, however, it partly imparts the character of an observable to the vibronic energy $E_{vib}{}^m$.* We will see, in the following, that this quantity can indeed typify real properties of LP species.

A more detailed outline of the shortly introduced vibronic model is given in the following section and elsewhere.[5,6]

As pointed out in the Introduction, the hardness rule is a significant outcome of the vibronic model and the supporting DFT calculations.[4,6,7] According to this rule, a complex or molecule becomes less susceptible to LP distortions the softer it is. Thus, although AX_3 molecules are generally found possessing the distorted C_{3v} structure, some AX_4^- and BX_4 species and even more AX_5^{2-}, BX_5^-, and CX_5 clusters remain in the T_d and D_{3h} parent geometries. In the CN = 6 case, finally, the distorted geometries are rather the exceptions. Even most of the fluoride complexes and molecules ($A^{III}F_6^{3-}$, $B^{IV}F_6^{2-}$, $C^{V}F_6^-$, XeF_6) are expected to stay as regular octahedra with a spherically symmetric s^2-type LP.

The three highest-symmetry distortions for octahedral complexes and molecules resulting from the components (or linear combinations of these) of the two vibronically active τ_{1u} vibrations are sketched in Figure 1. (Only the O_h parent geometry is considered; the D_{3h} alternative, the trigonal prism, is rarely observed, occurring only in strongly covalent compounds and complexes with weak ligand−ligand repulsions.) Whereas the C_{3v} and C_{2v} geometries would correspond to the (pseudo) capped octahedron and the (pseudo) pentagonal bipyramid, respectively, in the VSEPR description, there is no alternative for the C_{4v}-distorted octahedron; the latter will be seen to play the most important role in the LP distortion processes, however.

II.2. The Vibronic Coupling Model—A New Recipe. Classical vibronic coupling studies of lone pair entities are based on the Herzberg−Teller expansion of the ground- and excited-state potential energy surfaces and their coupling to linear and quadratic terms in the nuclear coordinates;[18,19] here, the respective coupling constants can be adjusted to DFT results.[4,7] Such vibronic models are predictive but become highly parametrized in the case of polyhedra with higher CNs. Recently, we introduced an alternative, more straightforward approach based on Slater's transition-state theory.[20] This two-parameter model[5] has been applied to lone pair species with CNs = 4 and 5[6] and is also the method of choice in the present study. A brief outline is given in the following paragraphs.

In DFT, the energy of a given many-electron state stems from a calculation in which the electron density is approximated by considering the occupied spin−orbitals resulting from a self-consistent solution of the Kohn−Sham (KS) equations; thus, ground and excited states imply different sets of KS orbitals. However, there is a unique case in which the ground state and *one* excited state can be described in terms of a common set of KS orbitals, namely, within the TS (transition state) concept introduced by Slater.[20] The following recipe[5] is applied:

(17) Reinen, D.; Atanasov, M. *Comprehensive Coordination Chemistry II, Vol. 1 Fundamentals*; Lever, A. B. P., Ed.; Elsevier: New York, 2003; Chapter 1.35.

(18) Maaskant, W. J. A.; Bersuker, I. B. *J. Phys.: Condens. Matter* **1991**, *3*, 37.

(19) Bersuker, I. B.; Balabanov, N. B.; Pekker, D.: Bogge, J. E. *J. Chem. Phys.* **2002**, *117*, 10478.

(20) Slater, J. C. *Adv. Quantum Chem.* **1972**, *6*, 1.

(i) Half of an electron is transferred from the doubly occupied $(s + p_z)^2$ lone pair HOMO of the distorted geometry $(\epsilon_-)^2$ to the empty LUMO $\epsilon_+(p_z + s)$.

(ii) One calculates the self-consistent field energy of the resulting $(\epsilon_-)^{1.5}(\epsilon_+)^{0.5}$ TS configuration by DFT.

(iii) The Franck−Condon many-electron transition energy E_{FC} (Figure 2b) is approximated in a remarkably accurate way by the orbital energy difference:

$$E_{FC} = \epsilon_+ - \epsilon_- \tag{2}$$

(iv) One utilizes the KS wave functions φ_+ and φ_- by expressing these in terms of the $\varphi(s)$ and $\varphi(p_z)$ MOs of the (undistorted) parent polyhedron:

$$\varphi_- = c_1\varphi(s) - c_2\varphi(p_z)$$
$$\varphi_+ = c_2\varphi(s) + c_1\varphi(p_z)$$
$$c_1^2 + c_2^2 = 1 \tag{3}$$

The matrix of vibronic interaction:

$$\begin{bmatrix} E_g - E & N \\ N & E_e - E \end{bmatrix} \tag{4}$$

refers to *any point* of the ground- and excited-state potential surfaces, yielding the energies E_- and $E_+ = E_- + E_{FC}$ on diagonalization. The nondiagonal coupling energy N as well as the ground- and excited-state energies E_g and E_e in the matrix can be expressed as

$$N = c_1c_2E_{FC}$$
$$E_g = E_- + c_2^2E_{FC}$$
$$E_e = E_- + c_1^2E_{FC} \tag{5}$$

where the mixing coefficients c_1 and c_2 refer to the wave functions (eq 3), which characterize E_- and E_+ in the distorted geometry. Specifically choosing the geometric and energetic situations at the minimum position of the distorted polyhedron (upper index m), with the initial energy E_g^0 of the undistorted geometry as the zero point of the energy scale, we arrive at the following expressions for the vibronic energy increments introduced in eq 1:

$$E_{rf}^m \equiv E_g^m = E_-^m + c_2^{m2}E_{FC}^m \tag{6}$$

$$E_{vib}^m = c_2^{m2}E_{FC}^m \tag{7}$$

Such an energetic situation is depicted in Figure 2b; here, E_g^m is the energy afforded to distort the polyhedron, excluding the stabilization by vibronic coupling. We add that eqs 6 and 7 are valid for any stage of distortion (without index m; see eq 9).

Proceeding from monomeric octahedra to *symmetric* dimer clusters, we note that $\varphi(s)$ and $\varphi(p_z)$ now transform to $\varphi(s_1) \pm \varphi(s_2)$ and $\varphi(p_{z1}) \pm \varphi(p_{z2})$ linear combinations. In addition, s_1 and p_{z1} (and similarly, s_2 and p_{z2}) functions mix in the lower (single octahedron) site symmetry (C_{4v}, C_{2v}, and C_{3v} for corner, edge, and face sharing, respectively; Figure 1) even if the bond distances toward bridging and terminal ligands are equal (see below). Taking, as an example, a face-sharing geometry, Z_2X_9 (see Figure 9a), the HOMO and LUMO functions of local C_{3v} symmetry, $a_1(s, p_z)$ and $a_1(p_z, s)$, give rise to a_1'- and a_2''-type linear combinations in the D_{3h} point group of the dimer. Specifically for $(Te_2Cl_9^-)_s$ in the ground-state minimum, the TS {corresponding to a $[\varphi_-(a_1')^{1.5}\ \varphi_-(a_2'')^{1.5}\ \varphi_+(a_1')^{0.5}\ \varphi_+(a_2'')^{0.5}]$ configuration} is characterized as follows (energies in eV), with the ligand contributions to the wave functions not listed:

$$\epsilon_-(a_1') = -7.427$$
$$\varphi_-(a_1') = -0.676(1/\sqrt{2})(s_1 + s_2) - 0.098(1/\sqrt{2})(p_{z1} - p_{z2}) + ...$$

$$\epsilon_+(a_1') = -3.933$$
$$\varphi_+(a_1') = -0.285(1/\sqrt{2})(s_1 + s_2) + 1.080(1/\sqrt{2})(p_{z1} - p_{z2}) + ...$$

$$\epsilon_-(a_2'') = -7.695$$
$$\varphi_-(a_2'') = 0.575(1/\sqrt{2})(s_1 - s_2) + 0.176(1/\sqrt{2})(p_{z1} + p_{z2}) + ...$$

$$\epsilon_+(a_2'') = -4.017$$
$$\varphi_+(a_2'') = -0.318(1/\sqrt{2})(s_1 - s_2) + 1.139(1/\sqrt{2})(p_{z1} + p_{z2}) + ...$$

Choosing the linear combinations

$$\epsilon_-^1 = (1/2)[\epsilon_-(a_1') + \epsilon_-(a_1'')] \qquad \varphi_-^1 = (1/\sqrt{2})[\varphi_-(a_1') - \varphi_-(a_2'')]$$

$$\epsilon_+^1 = (1/2)[\epsilon_+(a_1') + \epsilon_+(a_1'')] \qquad \varphi_+^1 = (1/\sqrt{2})[\varphi_+(a_1') + \varphi_+(a_2'')]$$

one obtains a pair of HOMO and LUMO functions dominated by either one of the two constituting octahedra:

$$\epsilon_-^1 = -7.561 \qquad \varphi_-^1 = -0.625s_1 - 0.137p_{z1} + ...$$

$$\epsilon_+^1 = -3.975 \qquad \varphi_+^1 = -0.301s_1 - 1.110p_{z1} + ...$$

where the negligible contributions from s_2 and p_{z2} (mixing coefficients < 0.05) are omitted. By such a procedure, we derive effective values for E_-, E_{vib}, and E_{rf} pertaining to one LP unit within the dimeric cluster. For the purpose of relating the Z_2X_9 cluster with an isolated ZX_6 complex, we chose, as the reference geometry and zero-point of the energy scale, the dimer with equal distances to the bridging and terminal ligands (Figure 11a). The Franck−Condon energy E_{FC} and electronic stabilization energy E_- (without the energy of solvation) for the dimer have been divided by half in order to have a realistic comparison between the single octahedra within the dimeric cluster and the isolated polyhedron.

II. 3. Computational Details. The calculations have been performed using the Amsterdam Density Functional (ADF) program (releases 2002.03 and 2003.01), within the local density approximation (LDA; Vosko, Wilk, and Nusair parametrization of electron gas data) and including gradient corrections (Perdew−Wang 1991; PW91 functional).[21] We used the triple-ζ(TZP) basis set provided by the program database. For the charged clusters, a charge-compensating polarizable solvent continuum has been introduced by applying the conductor-like screening model (COSMO) implemented in the ADF. We adopted the dielectric constant of water ($\epsilon = 78.4$) with the solvent radius $R_{solv} = 1.4$ Å; the solvation radii (in Å) used for the atoms constituting the complexes and molecules under consideration are Sn, 2.70; P, 2.40; S, 1.70; F, 1.40; I, 1.98;

(21) Baerends, E. J.; Ellis, D. E.; Ros, P. *Chem. Phys.* **1973**, *2*, 41. te Velde, G.; Baerends, E. J. *J. Comput. Chem.* **1992**, *99*, 84. te Velde, G.; Bickelhaupt, E. M.; Baerends, E. J.; Fonesca Guerra, C.; van Gisbergen, S. J. A.; Snyders, J. G.; Ziegler, T. *J. Comput. Chem.* **2001**, *22*, 931−967.

Ge, 2.60; As, 2.46; Se, 2.53; Cl, 1.75; Xe, 2.64; In, 2.71; Sb, 2.67; Te, 2.74; Br, 1.85; and Bi, 2.88.

Geometry optimizations and frequency calculations were performed to characterize the octahedral clusters with respect to eventual instabilities along any vibronically active distortion paths of the symmetry-breaking stretching and bending modes of τ_{1u} type (Figure 1). Most polyhedra were calculated to be at stable minima in O_h symmetry. The ground-state potential surfaces were explored in terms of geometry optimizations within the C_{4v}, C_{2v}, and C_{3v} subgroups of O_h by systematically elongating one, two, or three bond lengths, respectively. The longer distances were arbitrarily chosen, whereas the shorter bond lengths and the bond angles were allowed to fully relax. Because gradients are more sensitive with respect to shorter rather than longer bond lengths, more precise optimized geometries are obtained.

To account for entropy contributions, the free enthalpy changes accompanying the $ZX_6 \rightarrow ZX_5 + X$, $Z_2X_{10} \rightarrow 2ZX_5$, $Z_2X_9 \rightarrow ZX_5 + ZX_4$, and $Z_4X_{16} \rightarrow 4ZX_4$ dissociations were calculated as well as the translational, rotational, and vibrational increments to the internal energy (U) and to the entropy (S).

The PJT-type treatment, as introduced in the preceding sections, allows easy access to the quantities $E_{rf}{}^{m}$ and $E_{vib}{}^{m}$ (eq 1) or E_{rf} and E_{vib} (eq 9). The used two-state model turned out to work reasonably well in most of the cases studied here.

III. The CN = 6 Isolated Polyhedra

From all investigated octahedral halide ($X^- = F$ to I) complexes $A^{III}X_6{}^{3-}$ (A^{III} = As to Bi), $B^{IV}X_6{}^{2-}$ (B^{IV} = S to Te), and $C^{V}F_6{}^{-}$ (C^{V} = Cl to I) and the XeF_6 molecule, only $As(Sb)F_6{}^{3-}$ and $SF_6{}^{2-}$ are calculated to undergo a LP distortion (fluoride species in all cases, as expected from the hardness rule). For the latter complexes, the dissociation enthalpy (or more precisely, the free energy), according to eq 8a, is negative, indicating a vibronic instability along the C_{4v} distortion path (Figure 1) and leading, supported by the ionic radii effect, to the complete ablation of one ligand.

$$ZF_6{}^{n-}(O_h) \rightarrow ZF_5{}^{(n-1)-}(C_{4v}) + F^- + \Delta H_s \qquad (8a)$$

$$ZF_6{}^{n-}(O_h) \rightarrow ZF_5{}^{(n-a)-}(D_{3h}) + F^- + \Delta H_s' \qquad (8b)$$

It should be noted that the entropy contributions $T\Delta S$ supplementing the enthalpy ΔH (from translation, rotation, and vibration) were estimated by DFT to be negative, amounting to about $-0.3(1)$ eV for the LP species in Table 1. They should fully (in solution) or partly (in the crystalline state) enter the energy balance, giving rise to negative Gibbs free energy changes ΔG not only for $As(Sb)F_6{}^{3-}$ but also for $SF_6{}^{2-}$.

As may be deduced from Table 1, the LP effect is the deciding attribute, however, because it is the vibronic stabilization $[E_{vib}{}^{m}]_5$ of the five-coordinate species ($D_{3h} \rightarrow C_{4v}$) that turns the positive $\Delta H_s'$ into negative ΔH_s enthalpies (eqs 8a and 8b) for the above-mentioned three complexes. The lower index s indicates that the DFT calculations have been performed in a solvent continuum, in order to approximately account for the charge compensation in real systems by counterions either in solution or in a crystal lattice. The electrostatic solvent contribution is considerable (Table 1) and strongly stabilizes the species with the highest anionic charge (see ΔH and $\Delta H'$ in comparison with ΔH_s and $\Delta H'_s$). Apparently, only the inclusion of solvent energies renders sufficient reliability to the DFT results, such that a comparison with real systems is possible. One further notices that just the species with the lowest $\Delta H_s'$ dissociation enthalpies undergo dissociation, but only if the vibronic energy $E_{vib}{}^{m}$ for the $D_{3h} \rightarrow C_{4v}$ conversion of the five-coordinate complexes is large enough ($[E_{vib}{}^{m}]_5 > \Delta H_s'$). This gives support to the view that the ionic radii effect is involved in addition to the vibronic driving force.

Table 1. Dissociation Enthalpies (in eV) for Fluoride Complexes with CN = 6, with (ΔH_s, $\Delta H_s'$; eq 8) and without (ΔH, $\Delta H'$) Solvent[a]

	ΔH_s [b]	$\Delta H_s'$ [b]	$[E_-{}^{m}]_5$	$[E_{vib}{}^{m}]_5$	ΔH	$\Delta H'$
As^{III}, F	−0.07	0.52	−0.18	0.89	−6.44	−6.26
					(6.37)	(6.73)
Sb^{III}, F	−0.05	0.62	−0.18	0.91	−5.70	−5.52
					(5.65)	(6.13)
Bi^{III}, F	0.49	0.66	0.35	0.55	−4.87	−5.22
					(5.36)	(5.88)
S^{IV}, F	±0.00	1.10	−1.08	1.56	−2.52	−1.43
					(2.52)	(2.53)
Se^{IV}, F	0.68	1.39	−0.56	1.08	−1.59	−1.02
					(2.27)	(2.41)
Te^{IV}, F	0.57	1.47	−0.68	1.14	−1.23	−0.55
					(1.80)	(2.02)
Cl^{V}, F	1.45	2.26	−0.80	1.08	3.68	4.49
					(−2.23)	(−2.23)
Br^{V}, F	1.49	2.11	−0.60	0.94	3.74	4.36
					(−2.25)	(−2.25)
I^{V}, F	1.82	2.78	−0.96	1.25	4.04	5.00
					(−2.22)	(−2.22)
Xe^{VI}, F	3.03	3.99	−0.89	0.98	10.35	11.24
					(−7.32)	(−7.25)

[a] The solvent energy contributions are listed in parentheses. Furthermore, the electronic stabilization energies $E_-{}^{m}$ and the vibronic energy increments $E_{vib}{}^{m}$ (eq 1; in eV) for the $D_{3h} \rightarrow C_{4v}$ interconversion of the five-coordinate species are given (see lower index). [b] The entropy increment $T\Delta S$ favors the dissociation ($\Delta G < \Delta H$), compare the text.

After all, we claim that the nonexistence of the complexes $As^{III}F_6{}^{3-}$, $Sb^{III}F_6{}^{3-}$, and $S^{IV}F_6{}^{2-}$ is, particularly in the Sb^{III} case, essentially a vibronic LP effect. Support comes from the observation that the corresponding complexes $GaF_6{}^{3-}$, $InF_6{}^{3-}$, and $SiF_6{}^{2-}$ lacking the LP do exist. All of the other species collected in Table 1 are expected by DFT to be undistorted.

We proceed by analyzing the potential energy curves of selected examples from Table 1 along the C_{4v}, C_{2v}, and C_{3v} distortion paths (Figure 1) in greater detail. Figure 3 illustrates that these curves—for the $SeF_6{}^{2-}$ octahedron, for example—are considerably flattened when switching from C_{3v}-type to C_{2v}-type and finally to C_{4v}-type ligand motions. Furthermore, it is striking that they become steeper if Se^{IV} is replaced by Ge^{IV} lacking the lone pair. This observation can be shown to originate from the vibronic nature of the LP effect. According to eq 9, equivalent to eq 1 but not characterizing a new minimum at a distorted geometry as in Figure 2,

$$E_{rf} - E_{vib} = E_- \qquad (9)$$

an E_{vib} energy increment is active as soon as the O_h parent symmetry is left; however, because $E_{rf} > E_{vib}$, the electronic energy E_- is positive in this case (Figure 3). δE_t differs from

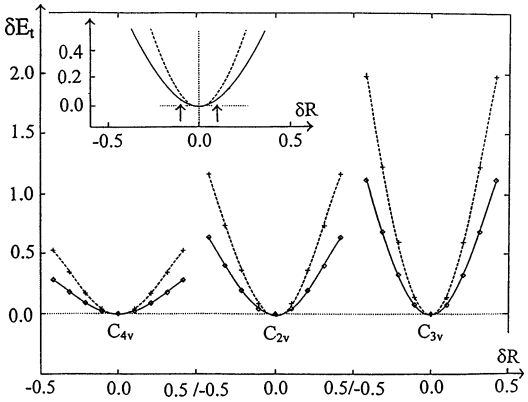

Figure 3. Potential energy curves of SeF_6^{2-} and GeF_6^{2-} (without the LP, dashed line) along the C_{4v}-, C_{3v}-, and C_{2v}-distortion paths. δE_t (in eV) is the total energy including the solvent energy (eq 10), and δR (in Å) is the increase of the bond length(s) in the LP direction (see Section II.3). In the C_{2v} inset, the experimental distortion δR of the SeF_6^{2-} polyhedron[12] (corresponding to $E_- \cong 0.04$ eV) is indicated.

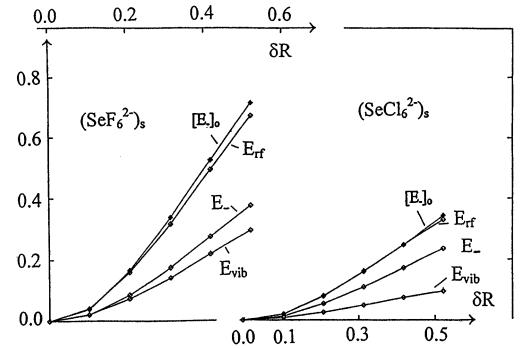

Figure 4. Correlation beween E_{rf}, E_{vib}, E_- (in eV), and the distortion parameter δR (C_{4v}) (in Å; elongation of the bond length in the LP direction) for the complexes $SeF(Cl)_6^{2-}$, in comparison to the dependence of $[E_-]_0$ for the corresponding $GeF(Cl)_6^{2-}$ complexes without LP on the same δR (C_{4v}) parameter.

E_- by additionally containing the electrostatic solvent contribution δE_s:

$$\delta E_t = E_- + \delta E_s \qquad (10)$$

In Figure 3, every point corresponds to a full DFT geometry and energy optimization at a given δR bond distance change. In Figure 4, left-hand side, the component energies E_{rf} and E_{vib} together with E_- (eq 9) are plotted with respect to δR (C_{4v}) for SeF_6^{2-} and compared with the E_- energy for $Ge^{IV}F_6^{2-}$ ($\equiv [E_-]_0$). It is striking that the latter energies are close to the restoring energies of the SeF_6^{2-} octahedron, this indeed demonstrating that it is the vibronic LP effect that flattens the potential curves by bringing E_{vib} into play (see below). The reported structure of the SeF_6^{2-} polyhedron in $(pip)_2SeF_6$ at 130 K[12] indicates a deformation "between C_{3v} and C_{2v}" with $\delta R \approx 0.10$ Å; there is a disorder in the triclinic unit cell of the space group $\bar{1}$ and with $Z = 1$, which suggests a dynamic distortion at higher temperatures. Such soft behavior indeed indicates a flat potential curve. Already small lower-symmetry strains by higher-order environmental effects[11] in a crystal structure may provide an energy stabilization of this magnitude. The SeF_6^{2-} polyhedron in $(pip)_2SeF_6$ cannot be considered as "naked"; presumably, hydrogen bonding imposes a strain of C_{3v} symmetry on the geometry in this case. Figure 4 finally illustrates that the vibronic energy increment E_{vib} is comparatively much smaller for $SeCl_6^{2-}$, well in accord with the hardness rule; again, E_{rf} for $SeCl_6^{2-}$ nearly matches the $[E_-]_0$ energy of the $GeCl_6^{2-}$ complex without the LP.

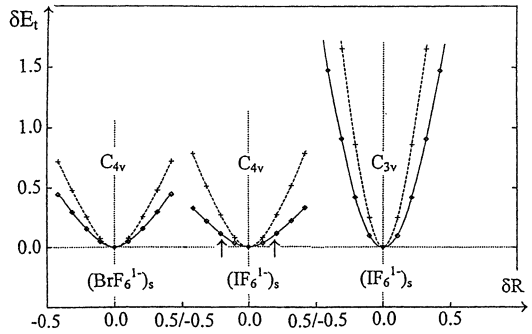

Figure 5. Potential energy curves of $I^VF_6^-$ and $Br^VF_6^-$ along the C_{3v}-, C_{4v}-, and C_{4v}-distortion paths, respectively, δE_t (in eV) versus δR (in Å), in comparison to those of $Sb^VF_6^-$ and $As^VF_6^-$ without LP (dashed line); the observed[14] deformation δR for the $I_2^VF_{12}^{2-}$ dimer ($\approx C_{4v}$; see Figure 7) is indicated.

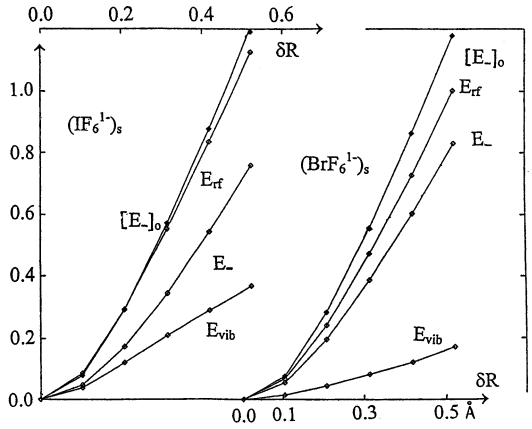

Figure 6. Dependencies of E_-, E_{rf}, and E_{vib} (eq 9; in eV) on the distortion parameter δR (C_{4v}) for the $I^V(Br^V)F_6^-$ complexes and the $[E_-]_0/\delta R$ correlation for the corresponding $(Sb^V)As^VF_6^-$ species without LP (δR in Å).

According to our calculations, the complex $Te^{IV}F_6^{2-}$, which has not been synthesized so far,[22] is expected to be stable as a regular octahedral species. However, the potential energy curves, particularly along the C_{4v} distortion path, are flat; the energy values collected in Table 1 suggest that the complex should be similarly strain susceptible to SeF_6^{2-}. Interestingly enough, a CN of 6 does exist in $[(C_2H_5)_4N]$-TeF_5,[16] where C_{4v}-distorted TeF_6^{2-} polyhedra are strain stabilized in $Te^{IV}{}_2F_{10}^{2-}$ dimers, as will be discussed in the following section (Figure 8b).

From the three complexes $C^VF_6^-$, the one with $C = I^V$ possesses the most-pronounced vibronic potential and that with Br^V the least-pronounced (see the $[E_{vib}^m]_5$ energies in Table 1). This is also clearly deduced from Figures 5 and 6, where selected potential energy curves [δE_t versus δR and correlations between E_-, E_{rf}, E_{vib}, and $\delta R(C_{4v})$] are depicted for $Br(I)F_6^-$. In correspondence with our results, a regular octahedral geometry is reported for $Cl^VF_6^-$ [13] and $Br^VF_6^-$,[12] whereas the considerable distortion in "$[(CH_3)_4N]I^VF_6$"[14]

(22) Moock, K. H.; Boeré, R. T. *J. Fluorine Chem.* **1994**, *68*, 175.

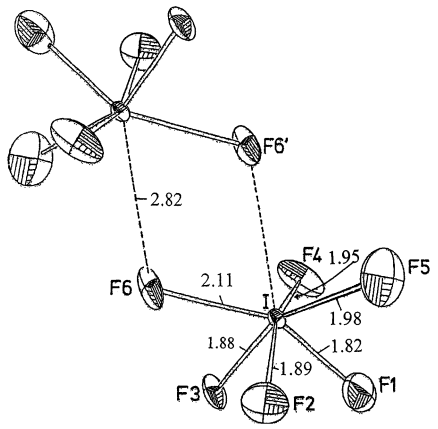

Figure 7. Geometry of the $I_2^{V}F_{12}^{2-}$ dimer in $[(CH_3)_4N]IF_6$ at 110 K (after[14]).

contrasts with these data at first sight. However, the mentioned salt contains dimers $I_2F_{12}^{2-}$ (Figure 7), with CN = 7 for each I^V center and two fluoride anions appearing as bridging ligands. We will see in the following section that *bridging* ligands possess a different binding capacity from that of *isolated* ones, thus imposing a pronounced lower-symmetry strain on each $[IF_5F_2']^{2-}$ complex (F′ = bridging ligand) and thereby activating the vibronic energy. Indeed, E_{vib} is largest for IF_6^-, as compared to ClF_6^- and BrF_6^- (Figure 6), and hence, particularly for this complex, the stabilization of a distorted geometry ($\approx C_{4v}$) is expected, in rather good agreement with Figure 7; a (bridging) ligand at 2.11 Å, close to the LP direction, here, a nearly opposite one at 1.82 Å and, finally, four equatorial ligands at ~1.93 Å occur. A stabilization energy of only about 0.08 eV would be sufficient to verify the experimental extent of distortion ($\delta R \sim 0.17$ Å). As in Figure 4, and in the cases of $Br^V(I^V)F_6^-$, the restoring energy E_{rf} equals (I^V) or is very near (Br^V) to the stabilization energy $[E_-]_0$ for the corresponding complexes $Sb^V(As^V)F_6^-$ without LP. This emphasizes, again, the significance of E_{vib} even for LP complexes, which are calculated to be stable as octahedral complexes in the absence of any strain due to lower-symmetry crystal forces or the presence of bridging ligands. One further significant result is that C_{4v} ligand motions afford much less energy than C_{2v}- and, finally, C_{3v}-type displacements (Figures 3 and 5), always for the same bond length expansion(s) in one (C_{4v}), two (C_{2v}), or three (C_{3v}) directions (Figure 1). One should further mention that the relation $E_{rf}(LP) \approx [E_-]_0(non\text{-}LP)$ is in no way generally valid. The example in Figure 2, above, illustrates that E_{rf}(LP) can be comparatively much smaller in the case of smaller CNs and pronounced LP distortions.

The δE_t versus δR potential curve (C_{4v} distortion path) of $Xe^{VI}F_6$ is calculated to be similar to that of $Br^VF_6^-$ (Figure 5). The reported C_{3v} distortion in the gas phase, deduced from electron diffraction and spectroscopic measurements, seems to be tiny and of a dynamic nature.[15] The apparent distortion along a trigonal axis may be looked at as the dynamic average over three C_{4v}-type motions. The latter ligand displacements are softer in our calculations than those along a 2-fold (C_{2v}) or 3-fold axis (C_{3v}), in contrast to suggestions,[15] which claim a reversed stability sequence of deformations, according to $C_{3v} > C_{2v} > C_{4v}$. Anyway, the geometric and energetic LP influence is only very small. The tetramers and hexamers found in the solid state, in which four and six fluoride anions, respectively, take over bridging functions, are composed of approximately C_{4v}-distorted octahedra, very similar to the $I_2^{V}F_{12}^{2-}$ dimer in Figure 7. Also here, the considerable vibronic energy E_{vib} (Table 1) can be activated by oligomerization, well in accord with our concept (see Section IV).

We mention here the results of two studies on octahedral LP fluoride species of the kind displayed in Table 1, utilizing more rigorous methods than DFT. Within a newly developed PJT-type approach, it is predicted[19] that XeF_6 is unstable with respect to τ_{1u} vibrations in O_h, whereas TeF_6^{2-} should stay undistorted, with IF_6^- being an intermediate case. On the other hand, sophisticated quantum-mechanical calculations[23] emphasize the difficulty in properly accounting for electron correlation and relativistic effects in determining the molecular geometry. The authors expect ClF_6^- and BrF_6^- to be undistorted species, whereas TeF_6^{2-}, IF_6^-, and XeF_6 should possess fluxional geometries along τ_{1u}-type pathways. For the particularly interesting, because it has not yet been synthesized, TeF_6^{2-} complex, there seems to be essential agreement with DFT; it is predicted to be vibronically stable but possibly posessing a flat potential energy surface.

IV. The CN = 6 Oligomers

As model oligomers, we have studied dinuclear complexes with one common edge (Figure 8) and one common face (Figure 9) and, furthermore, tetramers with the cubane structure (Figure 11). To detect the LP influence on the geometry of the constituting octahedra, we have always compared the structural data with those for corresponding oligomers without the LP.

IV.1. Dinuclear Species with One Common Edge. In Table 2, we have collected structural data of dinuclear complexes $A_2^{III}X_{10}^{4-}$ and $B_2^{IV}X_{10}^{2-}$ and molecules $C_2^{V}X_{10}$, giving also the enthalpies ΔH_s^D for the dissociation into two five-coordinate species $A^{III}X_5^{2-}$, $B^{IV}X_5^-$, and C^VX_5, respectively, with C_{4v} geometry. The symmetry of the dimers was, in the first instance, fixed at D_{2h}. It is striking to see that the C_{2v}-type distortion of the constituting octahedra, as measured by the bond length difference $r_b - r_t$ (Figure 8a), exceeds, by far, the one calculated for the respective species without LP, particularly in the case of the fluorides, whereas these differences are about equal in the case of the iodides, nicely following the hardness rule. The presence of a finite E_{vib} energy, activated by the symmetry lowering from O_h to C_{2v} according to the simultaneous presence of terminal and bridging halide ligands, is responsible for this enhancement of the distortion effect. Proceeding from X = F^- toward X = I^- reduces E_{vib} and, hence, the LP influence, the extent of the latter also somewhat depending on the central ions.

(23) Kaupp, M.; van Wüllen, C.; Frauke, R.; Schmitz, F.; Kutzelnigg, W. *J. Am. Chem. Soc.* **1996**, *118*, 11939.

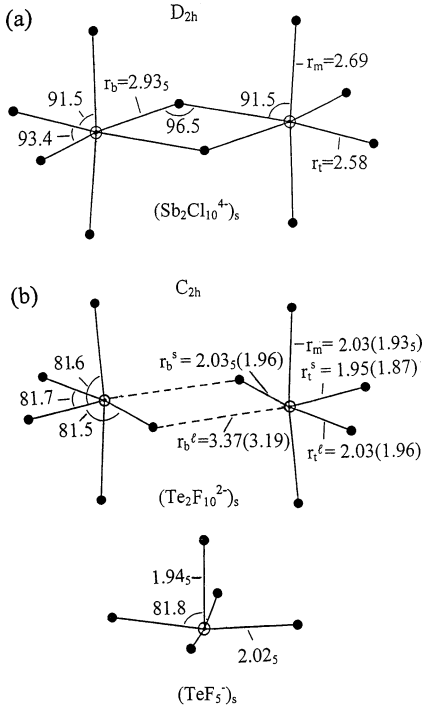

Figure 8. Calculated geometries (bond lengths in Å, angles in degrees) of dinuclear complexes with a common edge and central ions with one LP. $Sb_2^{III}Cl_{10}^{4-}$ with D_{2h} (a) and $Te_2^{IV}F_{10}^{2-}$ with C_{2h} symmetry (b) and symmetrical and asymmetrical bridgings, respectively, are the model examples. The values in parentheses in part b are experimental data;[16] the calculated structure of $Te^{IV}F_5^-$ is additionally depicted.

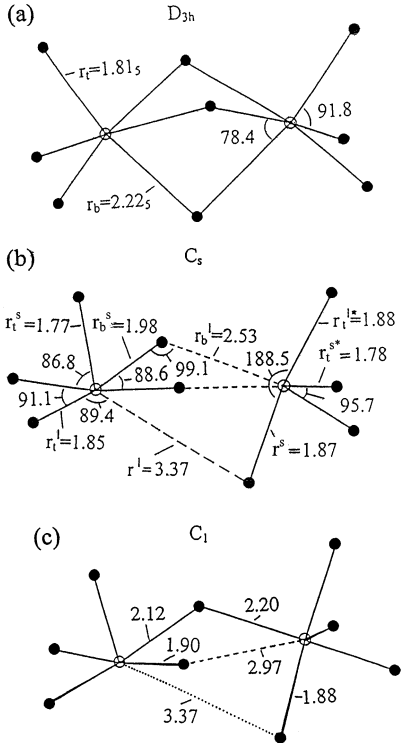

Figure 9. Calculated geometries (bond lengths in Å; angles in degrees) of the dinuclear complex $Se_2F_9^-$ with a common face between two octahedra for DFT optimizations in D_{3h} (a), in C_s (b), and—the absolute minimum—in C_1 (c).

Representative examples are the stable dimers $Sb_2^{III}Cl_{10}^{4-}$ (Figure 8a) and $Te_2^{IV}Cl(Br,I)_{10}^{2-}$, in comparison to the corresponding non-LP complexes with In^{III} and Sn^{IV}. Structural data[16,24] are mostly well in accord with the predictions from DFT (Table 2), within the limits of this approach, which systematically calculates the bond lengths to be too large, by about 4%.[4,6,7]

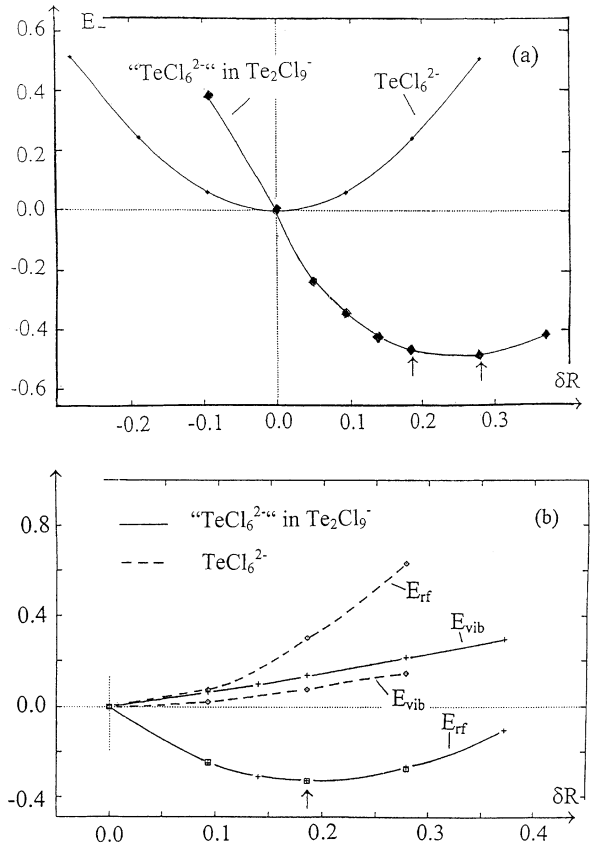

Figure 10. Correlations between the electronic energy E_-, the vibronic energy E_{vib}, the restoring energy E_{rf} (in eV), and the δR (C_{3v}) distortion parameter (in Å) for the constituting octahedra in the dinuclear complex $Te_2^{IV}Cl_9^-$, with a common face, and for the isolated $Te^{IV}Cl_6^{2-}$ octahedron. The arrows mark the DFT-optimized geometries for $Sn_2^{IV}Cl_9^-$ without the LP (δR = 0.19 Å), in parts a and b, and for $Te_2^{IV}Cl_9^-$ (δR = 0.28 Å) in part a; δR is the deviation of the long (bridging) bond lengths r_b (Figure 9a) from the octahedral bond distances, and the squares in the $E_{rf}/\delta R$ correlation of part b refer to the $[E_-]_0$ energies of the Sn^{IV} octahedra in $Sn_2Cl_9^-$.

Although, for all LP halide dimers with X = Cl^-, Br^-, and I^-, the enthalpy ΔH_s^D is positive, this is mostly not so in the case of the fluorides. The latter are not stable in D_{2h} but side-step into the lower-symmetry C_{2h} with an asymmetric bridge. The corresponding dimer geometry is shown in Figure 8b. Apparently, the vibronic energy is large enough to induce a local C_{4v}-type deformation instead of one with the less preferred C_{2v} symmetry. In the case of the $Sb_2^{III}F_{10}^{4-}$ dimer, the single-octahedron distortion of approximately C_{4v} symmetry even proceeds toward complete dissociation into two SbF_5^{2-} polyhedra. Because of the considerable energy gain for the $D_{2h} \rightarrow C_{2h}$ transformation ΔH_s^{DC} for the fluorides (Table 3), all dissociation enthalpies ΔH_s^C are now positive, reaching here the absolute energy minimum. In accord with the vibronic model, such geometry is indeed reported[16] for $Te_2^{IV}F_{10}^{2-}$, with bond lengths near to those calculated by

(24) Krebs, B.; Rieskamp, N.; Schäffer. A. *Z. Anorg. Allg. Chem.* **1986**, *532*, 118.

Table 2. Dinuclear LP Complexes $A_2^{III}X_{10}^{4-}$ and $B_2^{IV}X_{10}^{2-}$ and Molecules $C_2^{V}F_{10}$ with D_{2h} Symmetry (in Comparison to Corresponding Species with Non-LP Central Ions): Structural Data (see Figure 8a; in Å) and Enthalpies ΔH_s^D of Dissociation into Two Five-Coordinate C_{4v}- (or D_{3h}-) Type Species (in eV)

LP Complexes $A_2^{III}X_{10}^{4-}$ and $B_2^{IV}X_{10}^{2-}$				
X =	F^-	Cl^-	Br^-	I^-
		$Sb^{III}(In^{III})_2X_{10}^{4-}$		
r_t	2.07 (2.09_5)	2.58 (2.55_5)	2.76 (2.73)	3.02 (2.95_5)
$r_b - r_t$	0.50 (0.11)	0.36 (0.14_5)	0.29_5 (0.14_5)	0.23 (0.17_5)
r_m	2.17 (2.09)	2.69_5 (2.54)	2.85_5 (2.70_5)	3.10 (2.95)
ΔH_s^D	−0.51(0.58)	0.27 (0.13)	0.38 (−0.04)	0.40_5 (−0.04)
		$Se^{IV}(Ge^{IV})_2X_{10}^{2-}$		
r_t	1.83_5 (1.79)	2.32_5 [a] (2.28)	2.52 (2.47)	2.77 (2.73)
$r_b - r_t$	0.42_5 (0.20_5)	0.33[a] (0.27_5)	0.28 (0.26_5)	0.25 (0.27)
r_m	1.92 (1.78_5)	2.33[a] (2.29)	2.62 (2.48)	2.88_5 (2.76)
ΔH_s^D	−0.11 (0.27)	0.53 (−0.40)	0.56 (−0.44)	0.45 (−0.55)
		$Te_2^{IV}(Sn^{IV})_2X_{10}^{2-}$		
r_t	1.98_5 (1.98)	2.48[b] (2.44_5)	2.66_5 [c] (2.62_5)	2.94[d] (2.87_5)
$r_b - r_t$	0.42_5 (0.17)	0.37[b] (0.22_5)	0.31[c] (0.21_5)	0.28[d] (0.25)
r_m	2.05_5 (1.97)	2.58_5 [b] (2.45)	2.76[c] (2.63)	3.04[d] (2.89_5)
ΔH_s^D	−0.42 (1.02)	0.62_5 (0.18)	0.75 (0.07)	0.64 (0.04)
		Molecules $C_2^{V}F_{10}$		
		$Cl^V(P^V)_2F_{10}$		
r_t	1.70 (1.57)	$r_b - r_t$	0.42 (0.32_5)	
r_m	1.74 (1.58_5)	ΔH_s^D	-0.35_5 (−0.81)	
		$Br^V(As^V)_2F_{10}$		
r_t	1.81 (1.71_5)	$r_b - r_t$	0.37 (0.28_5)	
r_m	1.85 (1.72_5)	ΔH_s^D	0.01 (-0.02_5)	
		$I^V(Sb^V)_2F_{10}$		
r_t	1.93 (1.90)	$r_b - r_t$	0.40 (0.23)	
r_m	1.97_5 (1.90)	ΔH_s^D	−0.45 (0.77)	

[a] Experimental for r_t, $r_b - r_t$, and $r_m = 2.26(4_5)$, 0.40(18), and 2.37(3)[23], respectively (see text). [b] Experimental for r_t, $r_b - r_t$, and $r_m = 2.38_5(5)$, 0.44(22), and 2.50(2)[16], respectively (see text). [c] Experimental for r_t, $r_b - r_t$, and $r_m = 2.57$, 0.36, and 2.68,[16] respectively. [d] Experimental for r_t, $r_b - r_t$, and $r_m = 2.81_5(2_5)$, 0.31(8$_5$), and 2.94,[16] respectively.

Table 3. Geometric (Å) and Energy Data (eV) for Dimers $Se_2F_{10}^{2-}$ and $Cl(Br, I)_2F_{10}$ with C_{2h} Geometry (Figure 8b)[a]

	Se^{IV}	Cl^V	Br^V	I^V
r_b (D_{2h})	2.26	2.12	2.18	2.33
r_b^s	1.93_5	1.75	1.90_5	1.99_5
r_b^l	2.82	3.42	2.71	3.08
r_t^s	1.79	1.67_5	1.78	1.90
$r_m \cong r_t^l$	1.90_5	1.73	1.83_5	1.95_5
ΔH_s^C	0.12	0.07	0.17_5	0.24
ΔH_s^{DC}	−0.23	-0.42_5	-0.16_5	−0.69

[a] ΔH_s^C is the enthalpy of dissociation into two C_{4v}-type polyhedra with CN = 5, and ΔH_s^{DC} is the enthalpy for the $D_{2h} \rightarrow C_{2h}$ transformation. For $Te_2F_{10}^{2-}$ ($\Delta H_s^C = 0.13_5$; $\Delta H_s^{DC} = -0.55_5$ eV), see Figure 8b.

DFT (see Figure 8b). Though the geometries of the TeF_5^- dimer constituents are very near to those calculated for the isolated TeF_5^- polyhedra, the long bond of about 3.2 Å in the LP direction seems to be still energetically significant; the oligomerization process to the C_{2h} dimer is negative with -0.13_5 eV. Another example for a pronounced LP distortion of an octahedron, which is otherwise expected to be of O_h symmetry as an isolated entity, is $I_2^{V}F_{12}^{2-}$. Here, by the formation of two asymmetrically bridging ligands, a lower-symmetry strain is imposed on the two constituting IF_6^- octahedra, enhancing the local CN to 6 + 1 (Figure 7). A much less pronounced tendency toward the change from a symmetric to an asymmetric bridge (Figure 8) is also

Table 4. Dinuclear Complexes with a Shared Octahedral Face and D_{3h} Symmetry (in Comparison to the Corresponding Species without LP): Geometric Data (see Figure 9a; in Å) and Enthalpies ΔH_s^D (in eV) of Dissociation into One Five-Coordinate and One Four-Coordinate Polyhedron with C_{4v} (or D_{3h}) and C_{2v} (or T_d) Symmetry, Respectively

X =	F^-	Cl^-	Br^-	I^-
		$In_2X_9^{3-}$		
r_t	2.06	2.50	2.67	2.89_5
$r_b - r_t$	0.15_5	0.19_5	0.19_5	0.22_5
ΔH_s^D	1.12	0.21	−0.02	−0.34
		$Sb_2X_9^{3-}$		
r_t	2.09	2.56_5	2.74[a]	2.99_5
$r_b - r_t$	0.38_5	0.36	0.30_5 [a]	0.27
ΔH_s^D	-0.47_5	0.50	0.67	0.73
		$Ge_2X_9^-$		
r_t	1.73_5	2.23	2.42	2.67_5
$r_b - r_t$	0.25	0.28_5	0.28	0.29_5
ΔH_s^D	0.32	−0.92	−0.98	−1.25
		$Se_2X_9^-$		
r_t	1.81_5	2.30_5 [b]	2.49_5	2.75
$r_b - r_t$	0.41	0.35[b]	0.30	0.28
ΔH_s^D	0.04_5	0.95	0.87	0.60
		$Sn_2X_9^-$		
r_t	1.95	2.40_5	2.58_5	2.83_5
$r_b - r_t$	0.19_5	0.24	0.23_5	0.26
ΔH_s^D	1.41	0.05	−0.08	−0.36
		$Te_2X_9^-$		
r_t	1.98	2.46_5	2.64_5	2.92[c]
$r_b - r_t$	0.37_5	0.37_5	0.32_5	0.30_5 [c]
ΔH_s^D	-0.11_5	0.98	1.20	0.84

[a] Experimental for r_t and $r_b = 2.63$ and 3.00,[25] respectively. [b] Experimental for r_t and $r_b = 2.22(3)$ and 2.65(7),[16] respectively. [c] Experimental for r_t and $r_b = 2.80(4)$ and 3.13(5),[16] respectively.

predicted and observed (Table 2)[16,24] for some chloride dimers, according to the soft mode behavior of a specific β_{1g} vibration, which is involved in the $D_{2h} \rightarrow C_{2h}$ transformation. The structures of the series of dimers in ref 16 (p 250; Krebs et al.) nicely reflect this phenomenon induced by the preference of a C_{4v}-type local deformation to a C_{2v} distortion.

IV.2. Dinuclear Complexes with One Common Face. Tendencies similar to those in subsection IV.1 are found, if the dinuclear species contains a common face with symmetrical bridgings, thus imposing a strain of C_{3v} symmetry on each of the two constituting octahedra (Figure 9a). The structural and energetic data as calculated from DFT in Table 4 reflect that, again, the octahedron distortions, measured by the difference $r_b - r_t$ between the bridging and terminal bond lengths (Figure 9a), are considerably larger than those of the corresponding non-LP dimers, particularly in the fluoride cases, whereas the structural differences become very small for iodide as the ligand. Experimental examples[16,24] are mostly in satisfactory agreement with the calculations, within the limits of DFT. Also, for the dimers with a shared octahedral face, a strong tendency toward the formation of an asymmetric bridge is observed. Specifically in the case of the hard fluoride species, a distinct stabilization occurs (Table 5; $\Delta H_s^{DC} < 0$) if the dimer symmetry is lowered to C_s (Figure 9b). The enthalpy for the dissociation into two monomeric species [$Se_2^{IV}F_9 \rightarrow Se^{IV}F_5^-(C_{4v}) + Se^{IV}F_4(C_{2v})$, for example], which was negative for the D_{3h} dimer, is now positive (Table 5; $\Delta H_s^C > 0$). The symmetric bridge in D_{3h} is modified such that the left polyhedron now exhibits an

Table 5. Geometric (Å)[a] and Energetic (eV) Data for Dimers $Sb_2F_9^{3-}$ and $Se(Te)_2F_9^-$ with C_s Symmetry[b]

	r_t (6×)	$r_b{}^s$ (2×)	$r_b{}'$(2×)	r^s	r'	$\Delta H_s{}^C$	$\Delta H_s{}^{DC}$
$Sb_2F_9^-$	2.07(5)	2.15	3.14	2.09_5	3.53	0.06	−0.53
$Te_2F_9^-$	1.97(5)	2.07_5	2.79	1.99_5	3.66_5	0.59	−0.71

[a] For definitions, see Figure 9b; r_t is the average of the r_t' (2×), $r_t{}^s$, $r_t{}'$*, and $r_t{}^s$* (2×) bond lengths. [b] $\Delta H_s{}^C$ is the energy of dissociation into the monomeric 5- (C_{4v}) and 4-coordinate (C_{2v}) complexes, and $\Delta H_s{}^{DC}$ is the $D_{3h} \rightarrow C_s$ transition energy. The data for $Se_2F_9^-$ ($\Delta H_s{}^C = 0.43$; $\Delta H_s{}^{DC} = -0.38_5$ eV) are given in Figure 9b.

approximate C_{4v} distortion, whereas the right-hand side polyhedron shows a C_{2v} deformation; both phenomena are well in accord with the previously established sequence of increasing stability for distortions according to $C_{3v} \rightarrow C_{2v} \rightarrow C_{4v}$. The final DFT optimization in C_1, representing the absolute energy minimum for the dimers, is accompanied by only tiny additional enthalpy gains, ΔH ($C_s \rightarrow C_1$), smaller than 0.1 eV. Although the structure implies, particularly for $Sb_2{}^{III}F_9^{3-}$, already in C_s a stereochemistry rather near to the dissociation limit, with large $r_b{}'$ and r' distances (Table 5), in C_1 the "C_{2v}-type" bridge is further resolved, such that an approximately one-bridged dimer of C_{4v}-type Sb(Se, Te)F_5 square pyramids is formed (Figure 9c).

Without stressing finer structural details too much, we emphasize as the significant result that very pronounced LP deformations may appear in oligomers, even though the isolated octahedra are stable in O_h.

We will now investigate, in more detail, the physical origin of the strain influence on LP complexes, choosing $Te_2{}^{IV}Cl_9^-$(D_{3h}) as a representative example, by comparing either one of the two constituting octahedra of the face-connected dimer, $Te^{IV}Cl_3'Cl_3^{0.5-}$ (Cl′ = bridging ligand; see Figure 9a), with the corresponding isolated octahedron, $Te^{IV}Cl_6^{2-}$. In Figure 10a, the respective potential curves, the electronic energy E_- (eq 9) dependent on the previously (see caption Figure 3) defined distortion parameter δR along the C_{3v} ligand displacement path, are depicted; here, E_- for $Te^{IV}Cl_3'Cl_3^{0.5-}$ is taken as half of the dimer energy. The (relative) energetic zero point for the dimer octahedra is chosen for the geometry with $r_b = r_t$ and arbitrarily set equal to the potential energy minimum for the isolated complex. The arrows mark the δR values, which characterize the C_{3v} distortions of the Te^{IV} polyhedra (0.28 Å) and of the corresponding non-LP Sn^{IV} polyhedra (0.19 Å) in the respective dimers. The origin of the distortion enhancement in the LP case is revealed by Figure 10b, where again the energies, which refer to the dimers, are halved. The strain induced by the simultaneous presence of bridging and terminal ligands has a pronounced lowering impact on the restoring energy E_{rf}, which changes from positive for the isolated complex to strongly negative values for the dimer (Figure 10b). Also here, the $[E_-]_0$ energies of the non-LP dimer $Sn_2{}^{IV}Cl_9^-$ are nearly identical to the E_{rf} values of $Te_2{}^{IV}Cl_9^-$ (see the squares in the full-line E_{rf} curve of Figure 10b), with the minimum occurring at the δR value, which characterizes the distortion of the non-LP Sn^{IV} dimer (see arrow). Switching from the $Sn_2Cl_9^-$ to the $Te_2Cl_9^-$ dimer shifts the E_- potential energy minimum toward a distinctly

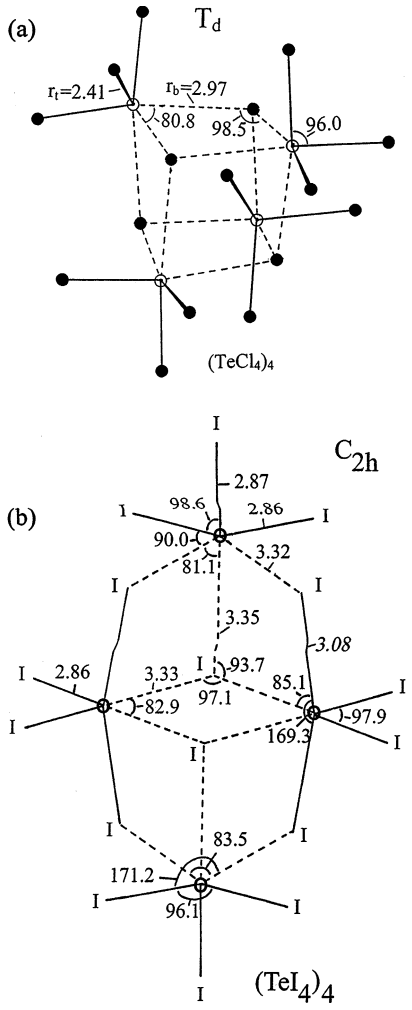

Figure 11. Cubane structure (T_d) of $(TeCl_4)_4$ (a) and the C_{2h} alternative for the $(TeI_4)_4$ tetramer (b).

larger distortion, though the respective energy gain is small (Figure 10a; -0.01_5 eV). After all, *the strain seems to predominantly affect E_{rf}, leaving E_{vib} essentially as it is in the case of the isolated octahedron*. It is the E_{vib} contribution, however, that displaces the potential energy curve to lower E_-energies at considerably higher δR parameters (vibronic enhancement). In the case of the isolated $TeCl_6^{2-}$ octahedron, the restoring energy E_{rf} is too large ($E_{rf} > E_{vib}$) to induce negative E_- energies, as noted before.

The role and the importance of external strains have been emphasized and thoroughly investigated, in particular, for chemical species underlying first-order Jahn Teller interactions by F. S. Ham.[26] Such strains are frequently significant when analyzing static distortions and the extent of these in Cu^{2+} chemistry.[27]

IV.3. Tetramers and Trimers. The halides (Cl^-, Br^-, and I^-) of S^{IV}, Se^{IV}, and Te^{IV} predominantly crystallize as tetramers with the cubane structure (T_d symmetry) in solid SCl_4, α- and β-$SeCl_4$, α- and β-$SeBr_4$, $TeCl_4$, $TeBr_4$, and

(25) Greenwood, N. N.; Earnshaw, A. *Chemistry of the Elements*; Butterworth/Heinemann: Oxford, 1998.
(26) Ham, F. S. *Electron Paramagnetic Resonance*; Geschwind, S., Ed.; Plenum Press: New York, 1972.
(27) Reinen, D.; Hitchman, M. *Z. Phys. Chem.* **1997**, *200*, 11.

Table 6. Structural Data (Å) for Cubane-Type Tetramers S_4X_{16} and Te_4X_{16} (as Compared to the Tetramer Sn_4X_{16} without LP) with T_d Symmetry (Figure 11a) and Dissociation Enthalpies ΔH^T [$B_4^{IV}X_{16} \rightarrow 4B^{IV}X_4$ with C_{2v} (T_d) Symmetry], in eV

X =	F	Cl	Br	I
		Sn_4X_{16}		
r_t	1.91_5	2.34_5	2.52_5	2.76_5
r_b	2.30	2.82_5	2.99_5	3.28_5
ΔH^T	0.69	−1.77	−1.92	−2.46
		Te_4X_{16}		
r_t	1.92_5	2.40_5[a]	2.59	2.86
r_b	2.51_5	2.97_5[a]	3.10_5	3.35_5
ΔH^T	0.51	2.42	2.74	1.48
		S_4X_{16}		
r_t	1.61_5	2.12_5	2.33	2.59_5
r_b	2.32	2.75	2.88	3.14_5
ΔH^T	−0.75	1.71	1.14	−0.15

[a] Experimental[16] for r_t and r_b = 2.31(1) and 2.93(3) Å, respectively.

ϵ-TeI_4 (metastable).[16] Here, a strain according to C_{3v} is imposed on each octahedron, and each of the three bridging ligands is involved in weak bonds to *three* central ions (Figure 11a). The selection of tetrameric clusters in Table 6 substantiates that the enthalpies of dissociation into four monomers with CN = 4 are (mostly) positive, confirming the experimental findings. In comparison, the corresponding non-LP tetramers are mostly highly unstable (the not-listed Si_4X_{16} entities to an even much larger extent than the Sn_4X_{16} tetramers). Here, the stability gain in the LP cases is also obviously enforced by the E_{vib} energy increment, which is activated by the low-symmetry strain due to the formation of ligand bridgings. A different geometric and energetic situation arises again for the fluorides, which are calculated to be more stable in symmetries lower than T_d. The DFT optimization in C_1 leads to drastic geometric and energetic changes in the case of S_4F_{16}, for example; the dissociation enthalpy ΔH^C is distinctly positive now (0.31_5 eV), and the structure corresponds to an assembly of very weakly interacting SF_4 molecules (via bridging distances ≥ 3.3 Å). This result is expected, keeping in mind that a $S^{IV}F_6^{2-}$ octahedron does not exist. In the case of Te_4F_{16}, a much more pronounced energetic stabilization occurs, with a dissociation enthalpy $\Delta H^C = 1.64_5$ eV. The interactions between the TeF_4 molecules in the low-symmetry C_1 assembly are distinctly stronger (bridging distances between 2.2 and 2.8 Å). Indeed, SF_4 and TeF_4 are reported[16] to possess a molecular C_{2v} geometry and a bridged chain structure, respectively.

Interestingly enough, the stable modifications of TeI_4 are reported to contain tetramers with the alternative structure, depicted in Figure 11b. DFT reproduces this result with an enthalpy $\Delta H^{TC} = -0.05$ eV for the $T_d \rightarrow C_{2h}$ transition. The average distortion of the constituting octahedra in the C_{2h} structure seems to be slightly smaller than that in the cubane alternative (Table 6; Figure 11b). One may speculate that the T_d tetrameric geometry becomes the less stable the smaller the vibronic energy is. Indeed, when inspecting the chloride cluster instead of the softer iodide tetramer, one obtains a positive enthalpy for the $T_d \rightarrow C_{2h}$ conversion ($\Delta H^{TC} = +0.11$ eV). Comparing, finally, the calculated bond lengths for Te_4I_{16} (Figure 11b) with the experimental ones for the δ- and γ-modification of TeI_4,[16] the agreement is again satisfactory, the calculated bond lengths being about 3% larger, well within the range of the usual deviation in our DFT optimizations. We refrain from going into further detail. It is our intention to reveal the essential features and trends of the LP interaction on a rather semiquantitative level, not overestimating the potential of the DFT approach in this respect.

An interesting oligomer, in which one fluoride ligand bridges three square-pyramidal IF_5 polyhedra via rather long I^V-F bond lengths of about 2.5 Å, is $I_3^VF_{16}^-$, a cluster in which every constituting octahedron undergoes a LP distortion toward C_{4v}. By DFT, a considerable stabilization energy is calculated for the trimer with respect to IF_6^-, if BrF_5 is used as a fluoride acceptor ($\Delta H_s = -0.75$ eV), in agreement with the observed direction of solvolysis (eq 11):[14]

$$3IF_6^- + 2BrF_5 \rightarrow I_3F_{16}^- + 2BrF_6^- \qquad (11)$$

$$IF_6^- + BrF_5 \rightarrow IF_5 + BrF_6^- \qquad (12)$$

A comparison with reaction 12, which has a positive enthalpy ($\Delta H_s = 0.33$ eV; see Table 1), again demonstrates that the formation of oligomers with bridging ligands may lead to a pronounced stabilization, induced by the activation of vibronic energy increments E_{vib}, if the symmetry is lowered. Though reaction 12 is reported[12] to pass from left to right, the stoichiometry might be obscured by the formation of oligomers such as in eq 11.

V. Summary and Conclusions

Simple group-theoretical considerations permit the specification of the active vibrational modes and, hence, the ligand displacement paths along which distortions from the high-symmetry parent structure to the lower-symmetry geometry occur as the consequence of the presence of a LP. In such a concept, it is the vibronic interaction between the electronic and ligand motions from which the driving force for a LP distortion and its energetic stabilization arises.[3] The vibronic coupling model developed on this basis has been successfully applied to account for the energetic and steric effect of halides and halide complexes of the fifth to eighth group elements with one LP, if supported by DFT. When following early ideas of R. G. Pearson,[8] the vibronic concept allowed the establishment of the *hardness rule*,[6,7] which correlates the tendency toward LP distortions with the chemical hardness. In particular, it is found that *the resistance toward LP deformations increases if the CN becomes larger*, this explaining why most octahedral LP complexes are stable in the high-symmetry parent geometry. In this study, we show, however, that even in such cases a vibronic energy potential is present, which flattens the potential energy curves along vibronically active ligand displacement paths as compared to the curves of corresponding chemical species without LP. In the following paragraphs, we summarize the most significant results.

1. The electronic energy E_-, which characterizes the potential energy curve of an octahedral complex, for example, can be considered to be composed of two incre-

ments: the restoring energy E_{rf} and the vibronic energy E_{vib} (eqs 1 and 9). The latter is a *pure binding contribution*, as emphasized elsewhere,[4,28] and comprises the contributions arising specifically from those orbital interactions, which are induced by the symmetry-lowering during distortion. E_{rf}, nearly always a positive quantity, approximately equals the electronic energy $[E_-]_0$ of the corresponding non-LP species in the here considered cases with CN = 6 (Figures 4, 6, and 10). After all, it is the orbital E_{vib} increment that finally stabilizes the LP distortion ($E_{vib} > E_{rf}$).

2. According to the DFT calculations within the vibronic model, octahedral halide complexes and molecules of the elements from the fifth to eighth main group with one LP should be stable in the O_h geometry, with the exception of some fluoride species, this trend following the *hardness rule*. Thus, $As^{III}F_6^{3-}$, $Sb^{III}F_6^{3-}$, and $S^{IV}F_6^{2-}$ are calculated to be unstable with respect to the C_{4v} distortion path to such an extent that the ligand in the LP direction completely leaves the complex. Although the nonexistence of the three mentioned complexes and the existence of undistorted $Cl^V F_6^-$ and $Br^VF_6^-$ polyhedra are well in accord with the predictions, the observed deformations of $Se^{IV}F_6^{2-}$, $Xe^{VI}F_6$, and $I^VF_6^-$ are unexpected from the standpoint of DFT at first sight. However, the LP deformations are small in the first two cases and most probably dynamic at 298 K, whereas in the third case, the considerably distorted polyhedron is not isolated; in the dimeric $I_2^VF_{12}^{2-}$ complex, two fluoride ligands are bridging (Figure 7), thus imposing a pronounced strain on the structure (see paragraph 3). It is further derived that the potential curves along a τ_{1u}-type distortion path (Figure 1) become distinctly flatter when proceeding from C_{3v} to C_{2v} and, finally, to C_{4v} deformations (Figures 3 and 5).

3. A low-symmetry external strain, imposed on a chemical species, may lower the restoring energy along the corresponding (τ_{1u} in the CN = 6 case) distortion path considerably, this leading to reduced or even negative E_{rf} values and, hence, to a potential energy minimum at a distorted geometry, usually even for non-LP species (Figure 11). The observed distortion of the corresponding LP complex or molecule, because of the presence of a finite E_{vib} energy, is much larger, however; the imposed distortion effect is *vibronically* enhanced. External strains can arise from the higher-sphere chemical environment of an isolated polyhedron in a crystal lattice[11] or, more effectively, by the presence of bridging ligands in oligomeric clusters, in addition to terminal ligands. We have particularly studied dimers and tetramers of such a kind (Figures 8, 9, and 11). There is a remarkable tendency for LP cations to form oligomers, which contrasts the tendency of the corresponding non-LP complexes, obviously as a result of the stabilizing presence of E_{vib} energy contributions. In the case of the hard fluoride ligands with a pronounced tendency to induce LP distortions, a trend to switch from local C_{3v}- and C_{2v}-type strains to strains with C_{4v} symmetry is predicted and, indeed, experimentally observed[16] (for example, $Te_2^{IV}F_{10}^{2-}$; Figure 8b).

The vibronic coupling model in combination with quantum-chemical calculations such as DFT has the potential to correctly account for the energetic and stereochemical anomalies connected with the presence of a LP. It is as illustrative as the VSEPR concept but goes beyond this model in its physical background and predictive power. We finally emphasize that the results and statements from the DFT-supported vibronic model are not claimed to be *quantitatively* correct. On the semiquantitative level, however, the conclusions and the predicted trends are in excellent agreement with available experimental evidence.

IC040125V

(28) Bersuker, I. B. *The Jahn−Teller Effect and Vibronic Interactions in Modern Chemistry*; Plenum Press: New York, 1984.